Vol 16 No 6, June 2007
1009-1963/2007/16(06)/1710-09
Chinese Physics
© 2007 Chin. Phys. Soc.
and IOP Publishing Ltd

Design and analysis of a novel single-mode single-polarization photonic crystal fibre based on polarization-dependent coupling and absorption effect*

Liu Xiao-Yi(刘小毅)†, Zhang Fang-Di(张方迪), Zhang Min(张 民), and Ye Pei-Da(叶培大)

Key Laboratory of Optical Communication and Lightwave Technologies, Ministry of Education, Beijing University of Posts and Telecommunications, Beijing 100876, *China*

(Received 25 June 2006; revised manuscript received 21 December 2006)

A novel single-mode single-polarization (SMSP) photonic crystal fibre has been proposed and analysed based on the polarization-dependent coupling and absorption effect via a full-vector finite element method with perfectly matched layers. The numerical results predict that very efficient SMSP operation can be achieved with both high bandwidth and high extinction ratio at low loss penalty. Effects of the fibre structural parameters on the SMSP bandwidth and extinction ratio have been explored, which will provide useful guide for the design and fabrication of the fibre. The results obtained will be instructive for the realization of new SMSP fibres with high performance.

Keywords: single-mode single-polarization (SMSP), photonic crystal fibre (PCF), finite element method

PACC: 4281, 4281D, 4281F, 0365D

1. Introduction

Single-mode single-polarization (SMSP) fibres, in which propagates one and only one polarization state of the fundamental mode, have recently been the subject of extensive experimental and numerical studies.[1−12] SMSP fibres can eliminate both polarization mode coupling and polarization mode dispersion, which is desirable for some polarization-sensitive applications such as high-power fibre lasers, fibre optic gyroscopes, current sensors and optical coherent communication systems.[12,13]

In the past years, most research efforts have been paid to the polarization maintaining fibres (PMFs) other than SMSP fibres since it is relatively more difficult to fabricate the latter. In general, to realize SMSP fibres, large birefringence is necessary to separate the two polarization modes, and what is more, a differential cutoff mechanism is needed to eliminate the unwanted polarization mode. Although SMSP fibres were first put forward in the 1980s,[14−20] the research in this area was not so active until the advent of photonic crystal fibres (PCFs) or hole-assisted fibres (HFs). PCFs possess many unusual optical properties like endless single-mode operation, highly tunable dispersion and highly controllable nonlinearity.[21,22] Highly birefringent PCFs have also been extensively studied, and the typical modal birefringence is on the order of 10^{-3} or even 10^{-2}, which is at least one order of magnitude larger than that of conventional PMFs.[23−27] This high birefringence is very helpful to realize high performance SMSP fibres. The potential of PCFs acting as SMSP fibres was first predicted by Steel *et al*[28] when considering the polarization properties of elliptical-hole PCFs. So far, various SMSP fibres utilizing PCFs or HFs have been proposed or demonstrated.[1−12] The large birefringence can be induced by geometric asymmetries,[1−4,6,9−11] or by stress effects,[5,7] or even by material anisotropies.[8]

It was predicted in the 1980s that the resonant absorption effect could be used to realize a SMSP fibre.[19] However, the author did not specify how to produce the large birefringence, and it seems difficult to fabricate this kind of multi-core fibre by the conventional techniques. In this paper, we propose a novel SMSP photonic crystal fibre based on polarization-

*Project supported by the National Natural Science Foundation of China (Grant Nos 60372100 and 60507007), and the State Key Development Program for Basic Research of China (Grant No 2003CB314906).
†E-mail: sliting@163.com

dependent coupling and absorption effect, for the first time to our best knowledge. An absorbent core with high material loss is introduced along the fibre to induce differential fundamental mode cutoff. The high index-contrast between air and silica glass with the highly flexible fabrication procedure permits large birefringence to be easily obtained in PCFs. Moreover, the stack-and-draw procedure of PCFs will make it straightforward to fabricate a multi-core fibre without any additional efforts.

A full-vector finite element method (FEM) with perfectly matched layers (PMLs) as the boundary condition is used to investigate the characteristics of the proposed fibre. Numerical results show that both high SMSP bandwidth and high extinction ratio can be achieved with proper design. And effects of the fibre structural parameters on the SMSP bandwidth and extinction ratio are explored.

2. Fibre structure and operation principle

Our proposed fibre consists of two parallel cores, and its cross structure is depicted in Fig.1(a). Due to the structure symmetry, only a half of the fibre cross section is presented. The fibre cladding is composed of triangular air hole lattice in pure silica background. A missing central air hole with two enlarged air holes defines the birefringent core A. The diameters of the cladding air holes and the enlarged air holes are denoted by d_1 and d_2 respectively. The air hole pitch is Λ. Meanwhile, a down-doped circular lossy core with high material loss and its surrounding six air holes define the isotropic and lossy core B. The diameters of the lossy core and its surrounding six air holes are denoted by d_4 and d_3 respectively. The distance between core A and core B is ρ. That is, core A is birefringent and lossless (no material loss), whereas core B is isotropic and highly lossy (large material loss). Figure 1(b) shows the equivalent refractive index distribution of the fibre along the x-axis.

The composite waveguide system can be viewed as two individual but coupled waveguides, and a similar system composed of two parallel slab nonidentical waveguides has been analysed using an improved coupled-mode theory.[29] However, a waveguide system with multiple parallel fibre cores can also be analysed by some numerical methods for the fibres with complex cross-section, such as effective-index method and finite element method (FEM).[20] In fact, a direct numerical mode solver seems more intuitive and effective in our case since it just provides the propagation constant and mode distribution that we are interested in. Using FEM, we have simulated a fibre structure with parameters $\Lambda = 3.3$ μm, $d_1/\Lambda = 0.40$, $d_2/\Lambda = 0.95$, $d_3/\Lambda = 0.565$, $d_4/\Lambda = 1.0$. The refractive indices of pure silica, air and down-doped lossy core are set at $n_s = 1.45$, $n_{\text{air}} = 1.0$ and $n_l = 1.448$, respectively. The choice of d_1 and d_2 is to produce large birefringence based on the structure asymmetry. The parameters of d_3 and n_l is properly adjusted to make the effective index of the isolated core B cross that of the isolated core A at a suitable wavelength. For convenience, we define this fibre as PCF1.

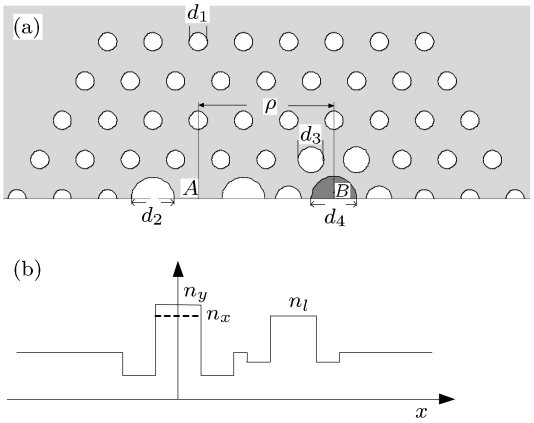


Fig.1. (a) Cross structure of the proposed fibre. (b) Equivalent index profile along the x-axis.

Before simulation, we assume that all the modes are x-polarized. Figure 2 plots the real part of the effective index $\text{Re}(n_{\text{eff}})$ as a function of wavelength for the modes supported by the isolated waveguides (core A and core B) and the two supermodes supported by the whole structure. The effective index of the first supermode is larger than that of the second one. For the first supermode, the effective index curve is core-A-like in the short wavelength region and becomes core-B-like with the increase of wavelength. The transition point is around the phase matching wavelength λ_{p} at which the propagation constants of the two modes supported by the two isolated waveguides (core-A and core-B) are equal. In other words, for the first supermode, when the wavelength is shorter than λ_{p}, light is mainly confined in core A; whereas, when the wavelength is longer than λ_{p}, light is mainly trapped in core B. However, things are totally converse when it comes to the second supermode, as shown in Fig.2. These

findings are in good agreement with those reported in Ref.[29]. The similar phenomena have been employed to design a dual-core dispersion-compensating photonic crystal fibre as in Ref.[30].

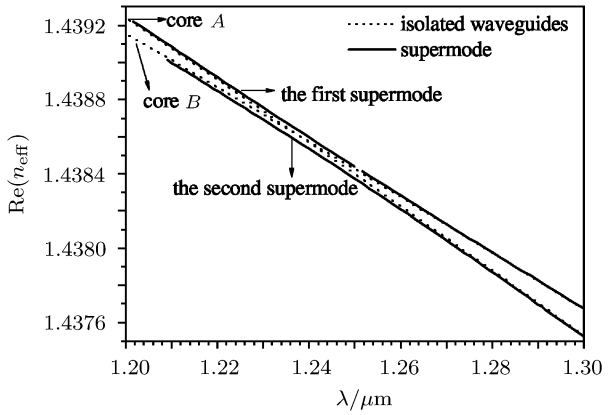


Fig.2. Effective index versus wavelength for the modes of isolated waveguides and supermodes.

At the phase matching wavelength, the first and the second supermodes can be equally excited and are responsible for the energy exchange between the cores A and B. However, at other wavelengths, there is nearly no energy exchange between the two cores due to the lack of phase matching.[31] In this case, the mode excitation is dependent on the light input. When the light is well input from core A, the first supermode is successfully excited, whereas the second one is very weak; however, when the light is well input from core B, the second supermode will be successfully excited, whereas the first one is very weak. In this paper, we must take care that the light should be well input from core A. To simplify the matter, we consider only the first supermode at the non-phase-matching wavelengths.

The mode characteristics of the y-polarized mode are similar to those of the x-polarized mode. However, because core A is highly birefringent while core B is isotropic, the phase matching wavelengths for the x- and y-polarized modes will be different. Therefore, when the operating wavelength lies between these two phase matching wavelengths (that means $\lambda_{{\rm p}x} < \lambda < \lambda_{{\rm p}y}$, where $\lambda_{{\rm p}x}$ and $\lambda_{{\rm p}y}$ represent the phase matching wavelengths for the x- and y-polarized modes respectively), if the mode is x-polarized, most of the energy will be trapped in the lossy core B and suffer from very high material absorption loss; however, if the mode is y-polarized, most of the energy is confined in the lossless core A and propagates along the fibre with low loss. Thus, large differential loss can be produced between the two polarization modes, and an efficient fibre polarizer can be obtained. In this paper, we call this the polarization-dependent coupling and absorption effect.

3. Modelling

FEM has been proved a very powerful, accurate and versatile tool for solving optical waveguide problems with the ability to deal with the waveguide cross section with arbitrary index distribution, which makes it very suitable for our case. A full vector model is necessary to accurately predict the propagation characteristics of PCFs due to the high index-contrast between air and silica glass. The Maxwell equation using electric field as a working variable can be expressed as

$$\nabla \times ([\mu_{\rm r}]^{-1}\nabla \times E) - \kappa_0^2[\varepsilon_{\rm r}]E = 0\,, \qquad (1)$$

where κ_0 is the free-space wavenumber, E denotes the electric field, and $[\varepsilon_{\rm r}]$ and $[\mu_{\rm r}]$ are the relative dielectric permittivity and magnetic permeability tensors, respectively.

In our simulation, a complex FEM modal solver for optical waveguides with PML boundary conditions is used to investigate the propagation characteristics of the proposed fibre such as effective index and mode field distribution.[32] The solution domain is divided by rectilinear triangular mesh elements, and the structure symmetries are exploited to save computation efforts and reduce the necessary memory. The element model we use is the hybrid edge/nodal element composed of the basic constant tangential and linear normal (CT/LN) vector basis functions with three tangential variables E_{t1}, E_{t2} and E_{t3}, and a linear nodal (conventional Lagrange) element with three axial variables E_{z1}, E_{z2} and E_{z3},[33] as shown in Fig.3. Applying the standard full vector finite element procedure yields a complex generalized eigenvalue equation[32]

$$[K]\{E\} = \kappa_0^2 n_{\rm eff}^2[M]\{E\}, \qquad (2)$$

where $[K]$ and $[M]$ are the finite element matrices, $\{E\}$ is the discretized electric field vector consisting of the edge and nodal variables, $e_{\rm eff}$ is the complex effective index.

This equation can be solved by means of high performance algebraic solvers. And the necessary memory can be significantly reduced by utilizing the sparsity of the matrix. Finally, we can obtain the complex effective index of the fundamental mode and the

mode field distribution. The modal birefringence can be simply calculated using

$$B = |\mathrm{Re}(n_{\mathrm{eff}}^{y}) - \mathrm{Re}(n_{\mathrm{eff}}^{x})|, \tag{3}$$

where n_{eff}^{y} and n_{eff}^{x} are the complex effective indices of the $y-$ and $x-$polarization modes respectively, and Re represents the real part.

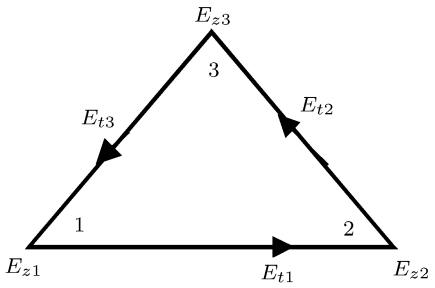


Fig.3. Hybrid edge/nodal element.

Suppose the material loss of the down-doped cores is γ_s, then the mode loss γ can be simply expressed as[20]

$$\gamma = \gamma_s P_s, \tag{4}$$

where P_s is the fraction of the mode power in the lossy region, here we define it as the normalized mode loss coefficient ($0 < P_s < 1$). P_s can be simply evaluated by

$$P_s = \frac{\iint_{\Omega} |E|^2 \mathrm{d}x\mathrm{d}y}{\iint_{s} |E|^2 \mathrm{d}x\mathrm{d}y}, \tag{5}$$

where Ω represents the lossy region, and s represents the whole fibre cross section.

4. Simulation results and discussion

4.1. mode field distribution

To demonstrate how the mode field distribution varies with the wavelength and polarization state, we have simulated the fibre PCF1.

First, we consider core A and core B separately. With core B ignored, core A is highly birefringent, and the effective indices versus wavelength for the x- and y-polarization fundamental modes are plotted as the dashed and solid lines in Fig.4(a) respectively. The modal birefringence of core A is on the order of $10^{-4} - 10^{-3}$, as shown in Fig.4(b), which is very helpful to yield a high bandwidth SMSP operation. With core A ignored, core B is isotropic, and the effective index for the degenerate fundamental mode supported by core B is plotted against wavelength as the dotted line shows in Fig.4(a). The cutoff wavelength of the fundamental mode (core A) is determined when the effective refractive index crosses that of the lossy core B at phase-matching wavelength. The difference in wavelength between the phase matching wavelengths of the two fundamental polarization modes is defined as the SMSP bandwidth.

As depicted in Fig.4(a), the phase matching wavelength of the x-polarization mode is about 1.24 μm, however, for the y-polarization mode, the phase matching wavelength is about 1.67 μm. Therefore, the fibre can operate as a SMSP fibre within the range from 1.24 to 1.67 μm and the SMSP bandwidth is as high as 430 nm.

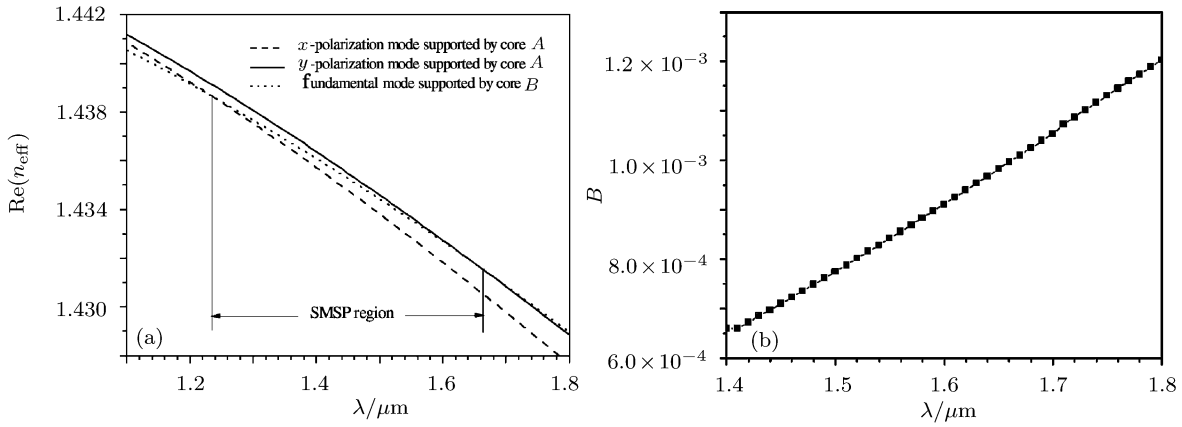


Fig.4. (a) Effective index versus wavelength for the fundamental mode supported by core A and core B. (b) Modal birefringence of core A.

The evolution of the mode field of the fundamental mode is depicted in Fig.4 at different wavelengths and in different polarization states. At wavelength shorter than λ_p, the field is essentially confined to core A, as shown in Fig.5(b). Around λ_p, optical coupling between core A and core B takes place, as shown in Fig.5(c). In fact, if the wavelength is exactly equal to λ_p, then core A and core B will be in resonance and the energy swaps back and forth between core A and core B, i.e., the energy is equally distributed between core A and core B. When the wavelength is longer than λ_p, however, most part of the fundamental mode spreads to core B and is effectively trapped in core B, as shown in Figs.5(a) and 5(d). It is observed clearly that when $\lambda = 1.55$ μm, the field of the x-polarization mode is mostly trapped in the lossy core B, whereas the y-polarization mode is effectively confined in core A. Thus, an efficient SMSP fibre is produced.

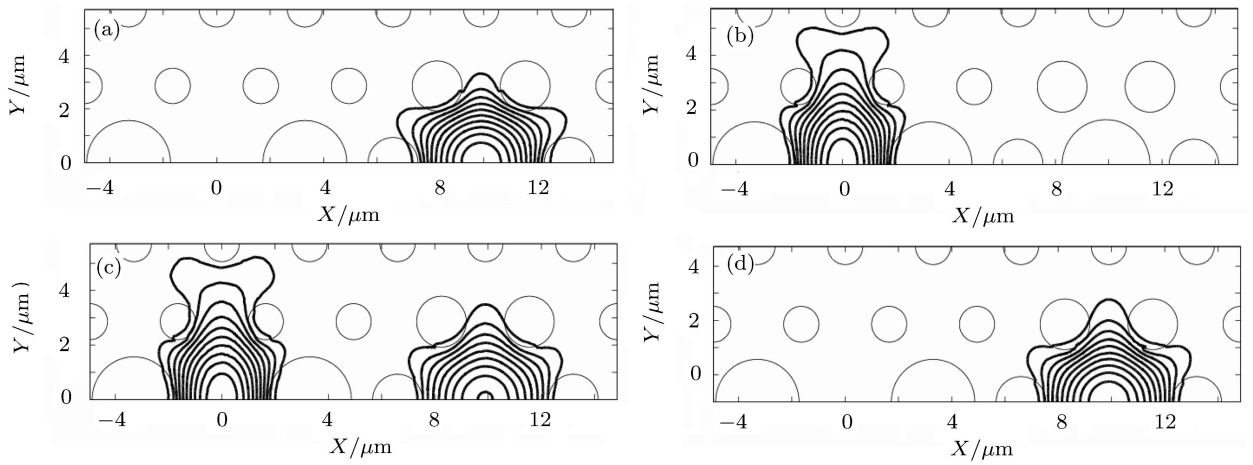


Fig.5. Evolution of the mode field of the fundamental mode at different wavelength and in different polarization states; (a) $\lambda = 1.55$ μm, x-polarization, (b) $\lambda = 1.55$ μm, y-polarization, (c) $\lambda = 1.66$ μm, y-polarization, (d) $\lambda = 1.75$ μm, y-polarization.

4.2. Extinction ratio

To determine the ability of the fibre to eliminate the unwanted polarization mode at a given penalty and over a certain distance, it is necessary to calculate the extinction ratio ER. In this paper, the y-polarization mode is guided while the x-polarization is eliminated. Assume the acceptable penalty loss for the guided $y-$polarization mode is α and the loss ratio of the two polarization modes is

$$\eta = \gamma_x/\gamma_y,$$

then in theory, the extinction ratio of the fibre can be expressed as

$$ER = \alpha \cdot (\eta - 1) \simeq \alpha \cdot \eta. \tag{6}$$

Thus, we should first obtain the propagation losses of the two polarization modes and then calculate the loss ratio η. In this paper, the polarization mode discrimination is mainly caused by the large differential material loss, hence we only consider the material absorption loss and neglect the confinement losses and any other losses. So, the mode loss can be normalized to the material loss through Eq.(4).

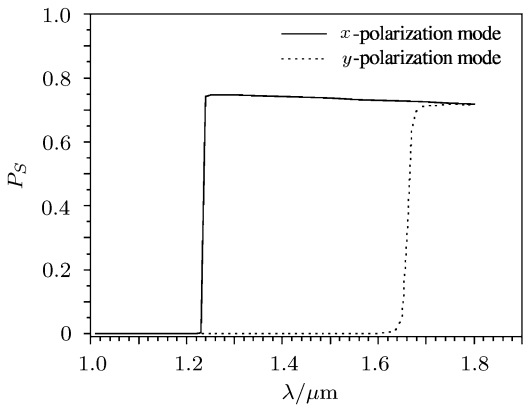


Fig.6. Normalized mode loss coefficient of both polarization modes as a function of wavelength for PCF1.

Consider the fibre PCF1. Figure 6 shows the normalized mode loss coefficient for the x- and y-polarization modes as functions of wavelength, respectively. In the short wavelength region, both the x- and y- polarization modes are well confined in core A, only a very small fraction of energy spreads to the lossy core B; however, when the wavelength increases to about 1.24 μm, most part of the x-polarization mode is

trapped in the lossy core B, and the normalized mode loss coefficient reaches about 75%.With the increase of the wavelength, as the mode confined in the lossy core B becomes more leaky, the normalized mode loss coefficient decreases gradually, i.e., more energy will spread into the surrounding silica glass and air hole claddings. On the other hand, within the wavelength range from 1.24 to 1.67 μm, the y-polarization mode is still well confined in the lossless core A. When the wavelength is longer than 1.67 μm, both the x- and y-polarization modes are trapped in the lossy core B.

Figure 7 plots the loss ratio of the two polarization modes as a function of wavelength for PCF1. The loss ratio peaks at wavelength 1.24 μm, with a value of 6.85×10^5. Then, with the increase of wavelength, the loss ratio decreases rapidly. This phenomenon can be interpreted by the following two facts: with the increase of wavelength, firstly, the energy of the x-polarization mode concentrated in the lossy region decreases since it becomes more leaky; and secondly, the energy of the y-polarization mode will spread more into the lossy region. It is clear from Fig.7 that if the loss ratio higher than 100 is required for SMSP operation, then within the wavelength range from 1.20 to 1.63 μm, the fibre can be viewed as a SMSP fibre. As a result, we obtain a very competent SMSP bandwidth as high as 430nm, which is almost twice of that obtained in Ref.[6].

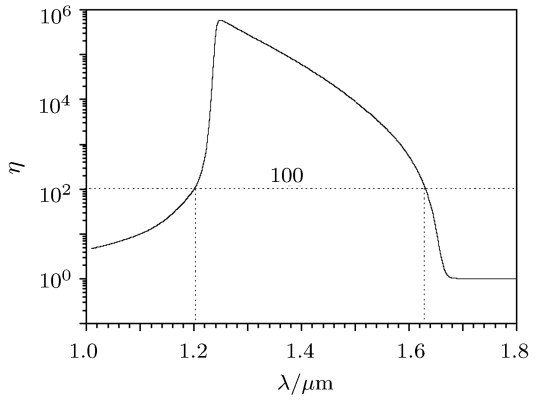


Fig.7. Loss ratio as a function of wavelength for PCF1.

From the loss ratio plotted in Fig.7, we can directly deduce the extinction ratio of the fibre at a given penalty and over a certain distance, through Eq.(6). For example, at wavelength 1.24 μm, the loss ratio is as high as 6.85×10^5, therefore, if the acceptable penalty loss for the propagation mode (y-polarization mode) is 0.01 dB/m, then the extinction ratio can reach about 6850 dB over one metre distance. At wavelength 1.55 μm, the loss ratio is about 2800, and if the acceptable penalty loss for the y-polarization mode is still 0.01 dB/m, then the extinction ratio can reach about 28 dB over one metre distance. This is a very efficient fibre polarizer. However, it should be clarified that we cannot expect the actual extinction ratio for a polarization mode to be higher than 40dB because of the random coupling induced by bending, stress, and thermal fluctuations.[17]

4.3. The location of the highly lossy region

At this point, we have demonstrated the fibre's ability to realize a SMSP operation with high bandwidth and high extinction ratio. Now, we begin to explore the effects of the structural parameters on the single polarization characteristics. To observe the effect of the highly lossy region's location on the single polarization characteristics, we calculate the loss ratio by changing the distance ρ while keeping the other parameters to be the same as PCF1.

The results are plotted in Fig.8 as a function of wavelength, which clearly shows that the loss ratio η increases significantly with the distance ρ. As ρ/Λ increases, the useful SMSP window is also broadened. That is, the farther the lossy region is placed from core A, the better is the polarization discrimination ability.

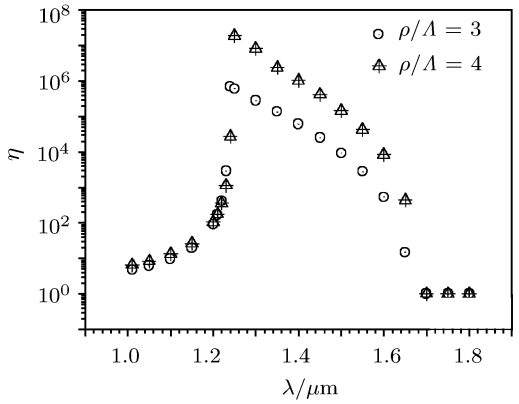


Fig.8. Loss ratio as a function of wavelength for different ρ/Λ.

4.4. The diameters of the six air holes surrounding the lossy region

Obviously, the fundamental mode cutoff and SMSP bandwidth are influenced significantly by the effective index of the fundamental mode supported by

the lossy core B, which is then determined by several factors, i.e. the size of the lossy region, the index of the lossy region, and the diameters of the six air holes surrounding the lossy region etc. In this paper, the diameter of the circular lossy region is fixed at $d_4/\Lambda = 1.0$. This arrangement can ensure most of the energy concentrated in the lossy region, and will facilitate the stack-and-draw procedure as well.

Figure 9 shows how the cutoff wavelength and SMSP bandwidth change as functions of the parameter d_3/Λ. The fibre parameters are kept the same as those for PCF1, except that d_3/Λ is set to be 0.560, 0.565, and 0.570 successively. It is clear from Fig.9 that the cutoff wavelength moves towards longer wavelength almost linearly as d_3/Λ increases. And the SMSP bandwidth increases monotonically with the increase of d_3/Λ. When d_3/Λ is set to be 0.560, 0.565, and 0.570, the SMSP bandwidths are about 335, 430, 500 nm, respectively.

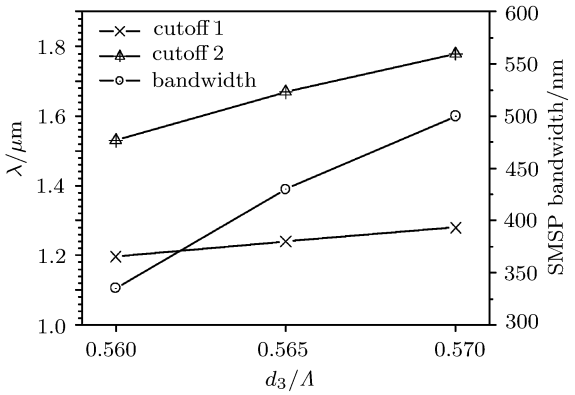


Fig.9. Cutoff wavelength of both polarization modes and the SMSP bandwidth as functions of d_3/Λ.

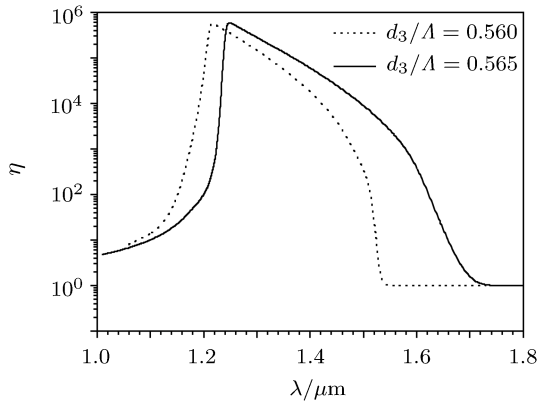


Fig.10. Loss ratio as a function of wavelength for different d_3/Λ.

The dependence of the loss ratio on d_3/Λ is depicted in Fig.10 as a function of wavelength. It reveals that the peak value of the loss ratio and the whole SMSP window shift to the short wavelength region, which confirm the results in Fig.9. In the long wavelength region, however, as both the x- and y-polarization modes are well confined in the lossy core, the loss ratio approaches to 1.0.

4.5. The refractive index of the lossy region

Another important parameter that can affect both the fundamental mode cutoff and the SMSP bandwidth is the refractive index of the lossy region. Figure 11 shows the cutoff wavelength and SMSP bandwidth as functions of the refractive index of the lossy region. The fibre parameters are the same as those in PCF1, except that the refractive index of the lossy region is changed from 1.4480 to 1.4483 with a step of 0.0001. The results show that the cutoff wavelength moves towards shorter wavelength almost linearly when the refractive index of the lossy region increases. The SMSP bandwidth decreases from 430 to 310nm when the refractive index of the lossy region increases from 1.4480 to 1.4483. That is, decreasing the refractive index of the lossy region is beneficial to yield a high SMSP bandwidth.

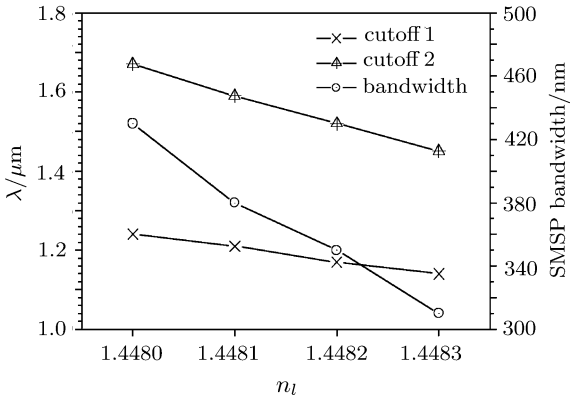


Fig.11. Cutoff wavelength of both polarization modes and the SMSP bandwidth as functions of the refractive index of the lossy region.

Figure 12 plots the loss ratio as a function of wavelength when the refractive index of the lossy region is set to be 1.4480,1.4481 and 1.4482 successively. The results show that the SMSP window shifts to the short wavelength region as the refractive index of the lossy region increases. Moreover, the peak value of the loss ratio increases with the increase of the refractive index of the lossy region. The mechanism behind this

is a little complicated. Firstly, the increase of refractive index of the lossy region will provide a stronger confinement for the trapped x-polarization mode, i.e., the x-polarization mode will suffer a little higher absorption loss. And secondly, since the coupling occurs at a shorter wavelength, less energy of the y-polarization mode can spread into the lossy region, i.e., the y-polarization mode will suffer lower absorption loss. Thus, the increase of the peak value of the loss ratio can be understood.

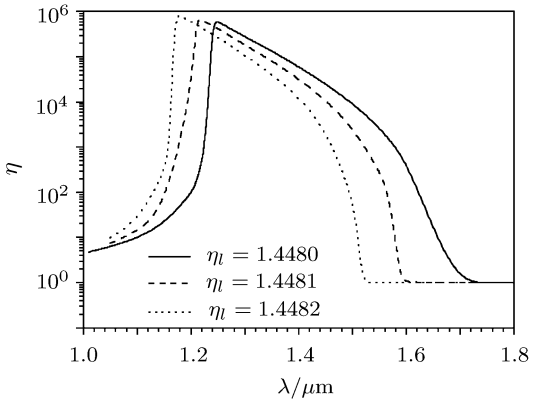


Fig.12. Loss ratio as a function of wavelength for different refractive index of the lossy region.

5. Tunability and fabrication considerations

From the analysis above, we can conclude that the refractive index of the lossy region can significantly tune the SMSP window and bandwidth. Therefore, if the refractive index of the lossy region can be tuned by voltage or temperature, it is possible to fabricate a SMSP fibre with tunable operating wavelength. Some materials like polymer or liquid crystal may meet the requirements.

The stack-and-draw procedure of PCFs will facilitate the fabrication of the fibre we proposed, the multi-core fibre can be fabricated without any additional efforts and the highly lossy region can be introduced by replacing a silica rod with a special rod made of highly lossy materials. It is essential to find suitable materials with compatible thermal and mechanical properties.

6. Conclusion

In this paper, we have proposed a novel SMSP photonic crystal fibre based on polarization-dependent coupling and absorption effect for the first time to our best knowledge. A full-vector FEM with PML boundary conditions is employed to investigate the propagation characteristics of the fibre. Numerical results predict that very efficient SMSP operation can be achieved with a bandwidth as high as about 500nm. And high extinction ratio can be obtained at very low penalty loss. From the analysis in all the sections above, we can draw some conclusions as follows:

1. The role of core A is to separate the two polarization states by producing large modal birefringence. In fact, we can also adopt other structures to produce the large birefringence.

2. The role of core B is to induce differential fundamental mode cutoff and absorb the energy of the unwanted polarization states. Depending on the material loss of the lossy region, high extinction ratio can be achieved at any given length of the fibre. Therefore, the present design would be suitable for both short- and long- distance applications.

3. The SMSP operation window and bandwidth can be tuned by the diameters of the six air holes surrounding the lossy region and the refractive index of this region. One can tune the operating wavelength to the desirable region by adjusting these two parameters.

4. The proposed fibre can be fabricated by the maturing stack-and-draw procedure of PCFs with properly selected materials.

In summary, the proposed SMSP PCF is very competent in terms of bandwidth and extinction ratio. The results obtained will be helpful for the design and fabrication of new SMSP fibres with high performance.

Acknowledgment

The first author Liu Xiao-Yi would like to thank professor Yu Chong-Xiu for her constant encouragement and kind support.

References

[1] Saitoh K and Koshiba M 2003 *IEEE Photon. Technol. Lett.* **15** 1384

[2] Kubota H, Kawanishi S, Koyanagi S, Tanaka M and Yamaguchi S 2004 *IEEE Photon. Technol. Lett.* **16** 182

[3] Lou S Q, Yan F P, Ren G B and Jian S S 2004 *Chin. Phys. Lett.* **21** 2448

[4] Nolan D A, Berkey G E, Li M J, Chen X, Wood W A and Zenteno L A 2004 *Opt. Lett.* **29** 1855

[5] Folkenberg J R, Nielsen M D and Jakobsen C 2005 *Opt. Lett.* **30** 1446

[6] Li M J, Chen X, Nolan D A, Berkey G E, Wang J, Wood W A and Zenteno L A 2005 *J. Lightwave Technol.* **23** 3454

[7] Schreiber T, Röser T, Schmidt O, Limpert J, Iliew R, Lederer F, Petersson A, Jacobsen C, Hansen K, Broeng J and Tünnermann A 2005 *Opt. Exp.* **13** 7621

[8] Zografopoulos D C, Kriezis E E and Tsiboukis T D 2006 *Opt. Exp.* **14** 914

[9] Ju Jian, Jin Wei and Demokan M S 2006 *J. Lightwave Technol.* **24** 825

[10] Zhang F D, Liu X Y, Zhang M and Ye P D 2006 *Acta Phys. Sin.* **55** 6453 (in Chinese)

[11] Liu X Y, Zhang F D, Zhang M and Ye P D 2007 *Acta Phys. Sin.* **56** 301 (in Chinese)

[12] Nolan D A, Li M J, Chen X and Koh J 2006 OFC OWA1. pdf

[13] Noda J, Okamoto K and Sasaki Y 1986 *J. Lightwave Technol.* **4** 1071

[14] Okoshi T and Oyamada K 1980 *Electron. Lett.* **16** 712

[15] Eickhoff W 1982 *Opt. Lett.* **7** 629

[16] Snyder A W and Riihl F 1983 *Electron. Lett.* **19** 185

[17] Okamoto K 1984 *Appl. Opt.* **23** 2638

[18] Okamoto K, Hosaka T and Noda J 1985 *J. Lightwave Technol.* **LT-3** 758

[19] Zheng X H 1988 *J. Lightwave Technol.* **6** 1265

[20] Chiang K S 1989 *J. Lightwave Technol.* **7** 436

[21] Russel P 2003 *Science* **299** 358

[22] Li S G, Liu X D and Hou L T 2003 *Acta Phys. Sin.* **52** 2811 (in Chinese)

[23] Ortigosa-Blanch A, Knight J C, Wadsworth W J, Arriaga J, Mangan B J, Birks T A and Russell P S J 2000 *Opt. Lett.* **25** 1325

[24] Hansen T P, Broeng J, Stig E B Knudsen E, Bjarklev A, Jensen J R and Simonsen H 2001 *IEEE Photon. Technol. Lett.* **13** 588

[25] Li S G, Xing G L, Zhou G Y and Hou L T 2006 *Acta Phys. Sin.* **55** 238 (in Chinese)

[26] Lou S Q, Ren G B, Yan F P and Jian S S 2005 *Acta Phys. Sin.* **54** 1229 (in Chinese)

[27] Lou S Q, Wang Z, Ren G B and Jian S S 2004 *Chin. Phys.* **13** 1052

[28] Steel M J and Osgood R M 2001 *J. Lightwave Technol.* **19** 495

[29] Shama Y, Hardy A A and Marom E 1989 *J. Lightwave Technol.* **7** 420

[30] Gérôme F, Auguste J L and Blondy J M 2004 *Opt. Lett.* **29** 2725

[31] Dietrich M 1987 *J. Lightwave Technol.* **LT-5** 113

[32] Saitoh K and Koshiba M 2002 *J. Lightwave Technol.* **38** 927

[33] Koshiba M,Tsuji Y 2000 *J. Lightwave Technol.* **18** 7